

We conclude that the Saturnian magnetoplasma interacted with the ionosphere-atmosphere system of Titan, leading to the formation of an induced magnetosphere and bipolar magnetic tail. This induced magnetosphere was observed to be deflected from the corotational flow direction and was also asymmetric with respect to the tail neutral sheet. Possible explanations include asymmetries of the atmosphere, finite gyroradius effects for the deflection, and a deviation from corotational flow. The upper limit for the magnetic moment of a possible internal magnetic field is 5×10^{21} gauss-cm³, consistent with at most a small convective, metallic core. This is, again, in agreement with the mean density and composition arguments.

NORMAN F. NESS

MARIO H. ACUÑA

RONALD P. LEPPING

JOHN E. P. CONNERNEY

KENNETH W. BEHANNON

LEONARD F. BURLAGA

Laboratory for Extraterrestrial Physics,
Goddard Space Flight Center
Greenbelt, Maryland 20771

FRITZ M. NEUBAUER

Technische Universität, Braunschweig,
Federal Republic of Germany

References and Notes

1. K. W. Behannon, M. H. Acuña, L. F. Burlaga, R. P. Lepping, N. F. Ness, F. M. Neubauer, *Space Sci. Rev.* **21**, 235 (1977).
2. M. H. Acuña, J. E. P. Connerney, N. F. Ness, *J. Geophys. Res.* **85**, 5675 (1980).
3. E. J. Smith, L. Davis, Jr., D. E. Jones, P. J. Coleman, Jr., D. S. Colburn, P. Dyal, C. P. Sonett, *ibid.*, p. 5655.
4. F. M. Neubauer, *Geophys. Res. Lett.* **5**, 905 (1978).
5. M. H. Acuña, F. M. Neubauer, N. F. Ness, *J. Geophys. Res.*, in press; F. M. Neubauer, *ibid.* **85**, 1171 (1980).
6. G. L. Siscoe, L. Davis, Jr., P. J. Coleman, Jr., E. J. Smith, D. E. Jones, *J. Geophys. Res.* **73**, 61 (1968).
7. B. U. Ö. Sonnerup and L. J. Cahill, Jr., *J. Geophys. Res.* **72**, 171 (1967).
8. J. H. Wolfe, J. D. Mihalov, H. R. Collard, D. D. McKibbin, L. A. Frank, D. S. Intriligator, *Science* **207**, 403 (1980).
9. H. S. Bridge *et al.*, *Science* **212**, 217 (1981).
10. J. Scudder, private communication.
11. N. F. Ness, *J. Geophys. Res.* **70**, 2989 (1965).
12. A. L. Broadfoot *et al.*, *Science* **212**, 206 (1981).
13. M. L. Kaiser, M. D. Desch, J. B. Warwick, J. B. Pearce, *Science* **209**, 1238 (1980); M. D. Desch and M. L. Kaiser, *Geophys. Res. Lett.* **8**, in press.
14. J. E. P. Connerney, M. H. Acuña, N. F. Ness, *J. Geophys. Res.* **86**, in press.
15. D. E. Jones, B. T. Tsurutani, E. J. Smith, R. J. Walker, C. P. Sonett, *J. Geophys. Res.* **85**, 5835 (1980).
16. We thank our colleagues in the Voyager Project, especially the Plasma Science Team (H. S. Bridge, principal investigator) for discussions of these early results, and the entire Voyager team at JPL for the success of this experiment. We also thank G. Sisk, E. Franzgrote, and M. DeGyurky of JPL for their support; C. Moyer, J. Scheifele, J. Seek, and E. Worley for contributions to the design, development, and testing at GSFC of the experiment instrumentation; and the data processing staff of the Laboratory of Experimental Physics at GSFC under the direction of W. Mish for their outstanding and dedicated support. One of us, F.M.N., was supported financially by the German Ministry of Science and Technology.

9 February 1981

SCIENCE, VOL. 212, 10 APRIL 1981

Plasma Observations Near Saturn:

Initial Results from Voyager 1

Abstract. Extensive measurements of low-energy plasma electrons and positive ions were made during the Voyager 1 encounter with Saturn and its satellites. The magnetospheric plasma contains light and heavy ions, probably hydrogen and nitrogen or oxygen; at radial distances between 15 and 7 Saturn radii (R_S) on the inbound trajectory, the plasma appears to corotate with a velocity within 20 percent of that expected for rigid corotation. The general morphology of Saturn's magnetosphere is well represented by a plasma sheet that extends from at least 5 to 17 R_S , is symmetrical with respect to Saturn's equatorial plane and rotation axis, and appears to be well ordered by the magnetic shell parameter L (which represents the equatorial distance of a magnetic field line measured in units of R_S). Within this general configuration, two distinct structures can be identified: a central plasma sheet observed from $L = 5$ to $L = 8$ in which the density decreases rapidly away from the equatorial plane, and a more extended structure from $L = 7$ to beyond 18 R_S in which the density profile is nearly flat for a distance $\pm 1.8 R_S$ off the plane and falls rapidly thereafter. The encounter with Titan took place inside the magnetosphere. The data show a clear signature characteristic of the interaction between a subsonic corotating magnetospheric plasma and the atmospheric or ionospheric exosphere of Titan. Titan appears to be a significant source of ions for the outer magnetosphere. The locations of bow shock crossings observed inbound and outbound indicate that the shape of the Saturnian magnetosphere is similar to that of Earth and that the position of the stagnation point scales approximately as the inverse one-sixth power of the ram pressure.

This is a preliminary report of the observations made by the plasma science experiment on Voyager 1 during the Saturn encounter period. The relevant instrument characteristics are discussed briefly in a report of the Jupiter encounter (1); a detailed description is available in (2). We discuss here (i) the bow shock and magnetopause crossings; (ii) the spatial distribution, composition, and flow of the magnetospheric plasma; (iii) the configuration of the plasma sheet; (iv) the interaction between Titan and the magnetospheric plasma; and (v) Titan and the atomic hydrogen torus as sources of plasma.

Boundary crossings. As Voyager 1 approached Saturn, a single bow shock

crossing was observed on 11 November 1980 at 2326 [all times in this report are spacecraft event times in universal time; and distances given in units of Saturn radii (R_S) refer to an equatorial radius of 60,330 km]. Five magnetopause crossings occurred between 0154 and 0248 on 12 November. The spacecraft remained inside the magnetosphere until 14 November, when it again crossed the magnetopause boundary five times and then reentered the interplanetary wind on 16 November (Table 1). The times of bow shock crossings (both inbound and outbound) compare well with those expected on the basis of a bow shock shape observed for Earth (3), the solar wind ram pressure (P), the position of the first

Table 1. Bow shock and magnetopause crossings and external wind parameters.

Boundary	Time*		Distance (R_S)
	<i>Inbound crossings</i>		
Shock	11 November	2326	26.1
Magnetopause	12 November	0154	23.6
		0213	23.4
		0228	23.2
		0242	22.9
		0248	22.7
	<i>Outbound crossings</i>		
Magnetopause	14 November	1729	42.7
		1806	43.4
		2034	45.7
		2115	46.1
		2140	46.9
Shock	16 November	0619	77.4
	<i>External solar wind parameters</i>		
	11 November: 420 km/sec, 0.11 cm^{-3} , flow from sun		
	16 November: 460 km/sec, 0.16 cm^{-3} , flow from 4° above ecliptic		

*Times are approximate entries into and exits from the magnetosheath and do not reflect the boundary layer phenomena which are observed.

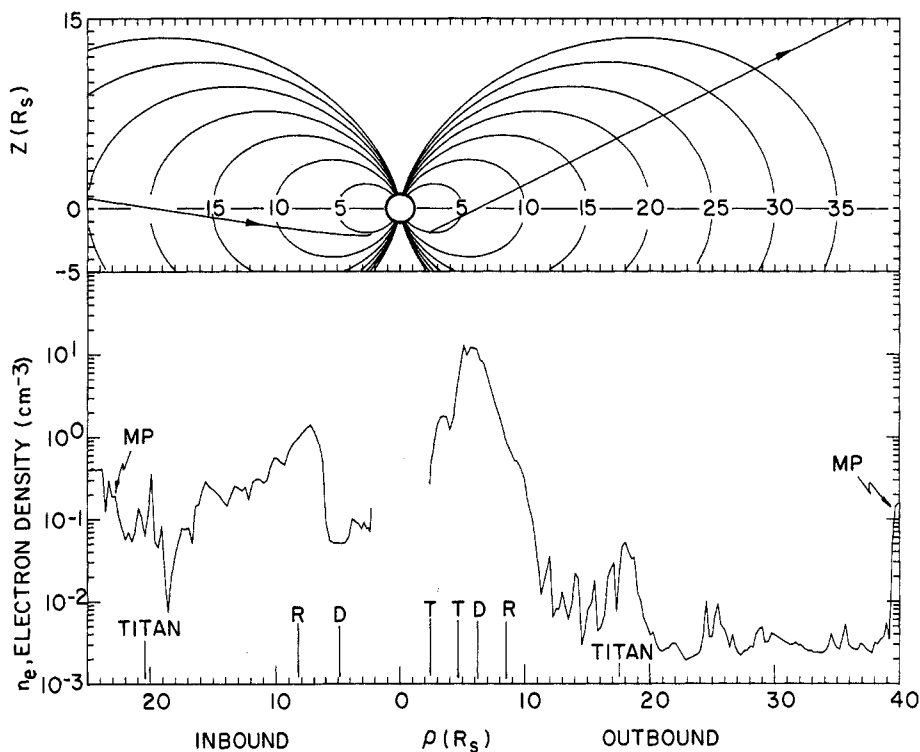


Fig. 1. Plasma electron densities (cm^{-3}) measured within Saturn's magnetosphere. The plotted points are 15-minute averages of electron measurements; ρ is the distance from Saturn's rotation axis. The upper panel shows the spacecraft position in the same coordinate system; Z is the distance from the equatorial plane. Dipolar field lines corresponding to indicated values of the flux tube parameter L are also shown. Values of ρ at which the spacecraft crossed the L shells of Titan, Dione (D), Rhea (R), and Tethys (T) are indicated above the abscissa of the lower panel. The last magnetopause crossing on the inbound portion of the trajectory and the first on the outbound portion are indicated by MP .

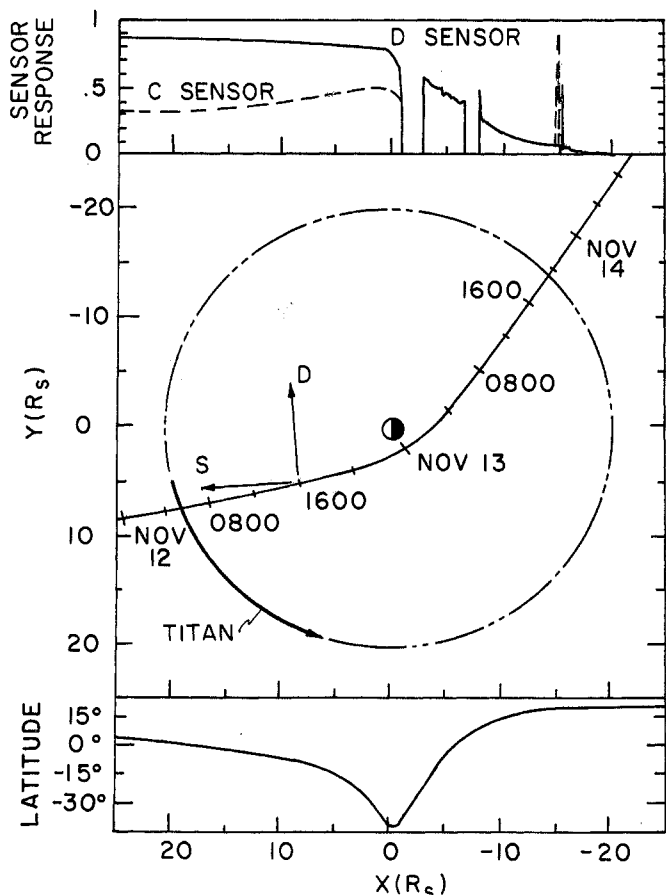


Fig. 2. The magnetospheric portion of the spacecraft trajectory projected onto Saturn's equatorial plane. The meridian plane, which passes through the sun, contains the x axis, which is positive toward the sun. The projection onto the equatorial plane of the symmetry axis of the plasma sensors which face Earthward (S) is shown as is the projection of the side sensor's look direction (D). The orbit of Titan is shown and its motion during the magnetospheric passage is indicated by the arrow. The lower panel shows the Kronographic latitude of the spacecraft. The upper panel shows the relative response of the D sensor and one of the Earthward-looking sensors to cold ions corotating with Saturn.

bow shock crossing observed by Pioneer 11 (4), and a shock distance proportional to $P^{-1/6}$. The location of the shock also agrees with that predicted from the shock shape and location at Earth and the pressure balance between the solar wind and a magnetic dipole of the strength observed at Saturn. Thus, Saturn's magnetosphere appears to be much less inflated by plasma than is Jupiter's. Nevertheless, the first magnetopause crossing on the inbound pass occurred at $23.6 R_S$, considerably earlier than expected from the location of the shock; at Earth, the ratio of shock to magnetopause distance is $\sim 4/3$. This discrepancy implies either that the solar wind pressure decreased by about a factor of 3 during the magnetosheath passage or that the ratio of shock to magnetopause distance is less than expected, perhaps because of large wave amplitudes in the magnetosheath or the presence of a Titan plasma torus.

Magnetospheric plasma observations.

We used electron rather than positive ion densities to define quantitatively the density profile of low-energy magnetospheric plasma at Saturn. Since low-energy electrons are essentially isotropic and constitute a single ionic species, this avoids complications that arise in interpreting positive ion measurements, namely, the presence of different ionic species, deviations from the corotational flow direction, and the sensor response as a function of Mach number. Details of the electron analysis, which self-consistently corrects for variations in spacecraft potential while the spacecraft remains illuminated in varying plasma conditions, have been extensively discussed for this instrument in connection with the reduction of electron data at Jupiter (5). The ion densities are in reasonable agreement with the electron densities reported below.

The close alignment of Saturn's rotation axis with its magnetic dipole axis (6, 7) suggests that the plasma observations in the Saturnian magnetosphere be presented in a cylindrical, Saturn-centered coordinate system aligned with the rotation axis, as done in Fig. 1 for the density data and spacecraft trajectory (upper panel). The principal features of the density plot in Fig. 1 are (i) the changes in density associated with magnetopause crossings between 23 and $25 R_S$ inbound and beyond $39 R_S$ outbound; (ii) the density spike associated with the Titan encounter near $20 R_S$; (iii) two regions of density enhancement during the inbound ($20 R_S$) and outbound (18 to $20 R_S$) passes, which suggest the presence of a plasma torus associated with Titan and

extending at least halfway around Saturn; (iv) an equatorially confined plasma sheet surrounding Saturn, indicated by the two broad density enhancements (17 to 6 R_S inbound and 3 to 11 R_S outbound); and (v) a low-density region during the outbound pass from beyond 20 R_S to the first magnetopause crossing outbound at 39 R_S . In that region, plasma densities range from 10^{-2} cm^{-3} to a few times 10^{-3} cm^{-3} .

In discussing the ion observations, it is necessary to keep in mind the orientation of the different look directions of the sensor during the encounter. Figure 2 shows the spacecraft trajectory and the viewing directions of the instrument projected onto Saturn's equatorial plane for the time interval covering the magnetospheric portion of the encounter.

The ion observations are characterized by relatively broad spectra and varying densities, but with periods of temperature low enough to allow the resolution of distinct peaks in the energy/charge spectra. Figure 3 shows a sequence of spectra measured by the D sensor, which looked nearly into the corotating flow during most of the incoming portion of the trajectory. Well-resolved spectral peaks are obtained for many observations during this interval; with these spectra, it is possible to calculate the component of corotational velocity along the D sensor normal; in the following discussion we refer to this component simply as "velocity." In Fig. 4, these estimated velocities are compared with the velocities expected if the magnetosphere were rigidly corotating at the rotational period obtained by the planetary radio astronomy experimenters (8). We assume that the lower energy peak is hydrogen and that the upper peak has a mass-to-charge ratio, A/Z^* , of 14 (A is atomic mass number and Z^* is effective charge number). These assumptions should be viewed as setting the approximate range of A/Z^* and not as identification of the ions. The velocities of the heavier and lighter components should coincide when proper identification has been made (9). Figure 4 shows generally good agreement in the velocities, with some notable exceptions that need further study. For example, from ~ 13 to $10 R_S$, the two velocities are brought into better agreement if $A/Z^* = 2$ is used for the lighter mass; thus we cannot exclude significant variations in the composition of the lighter component in this region of the magnetosphere. The best preliminary statement that can be made is that from ~ 7 to $\sim 15 R_S$ the corotation velocity is within 20 percent of that expected for rigid corotation

[compare with similar observations at Jupiter (9)].

Occasionally, the density is high enough and the temperature low enough to allow analysis of the observed currents with the narrower windows of the higher resolution mode. Figure 5 shows an example of such a spectrum and the analysis of the two peaks; a value of $A/Z^* = 1$ is assumed for the lower energy peak. In this case, the choice of $A/Z^* = 16$ for the heavier peak makes the resulting difference in velocities correspond to a slightly negative spacecraft potential, in disagreement with estimates of magnitude and sign from the electron analysis. On the other hand, if A/Z^* were

14, the potential would be positive and somewhat larger than that estimated by the electron analysis. Thus, at this preliminary stage in the analysis, it is possible to say only that the heavy mass has an A/Z^* in the range of 14 to 16 atomic mass units.

Figure 6 shows a sequence of D sensor spectra taken after closest approach as the spacecraft rises up to reencounter the equatorially confined plasma sheet. (As shown earlier, the D sensor faces into an unfavorable direction until the spacecraft rolls at about 0100.) Just after the roll, the peak of the low-energy portion of the plasma appears to be below the threshold energy/charge of 10 V, but

Fig. 3. Sequence of ion spectra taken from 0800 to 1216 on 12 November. The relative distribution functions observed from low-resolution mode measurements made by the side-looking (D) sensor plotted against energy/charge. The spectral points are interpolated by use of a cubic spline fit. The peaks corresponding to ions with different A/Z^* are clearly resolved.

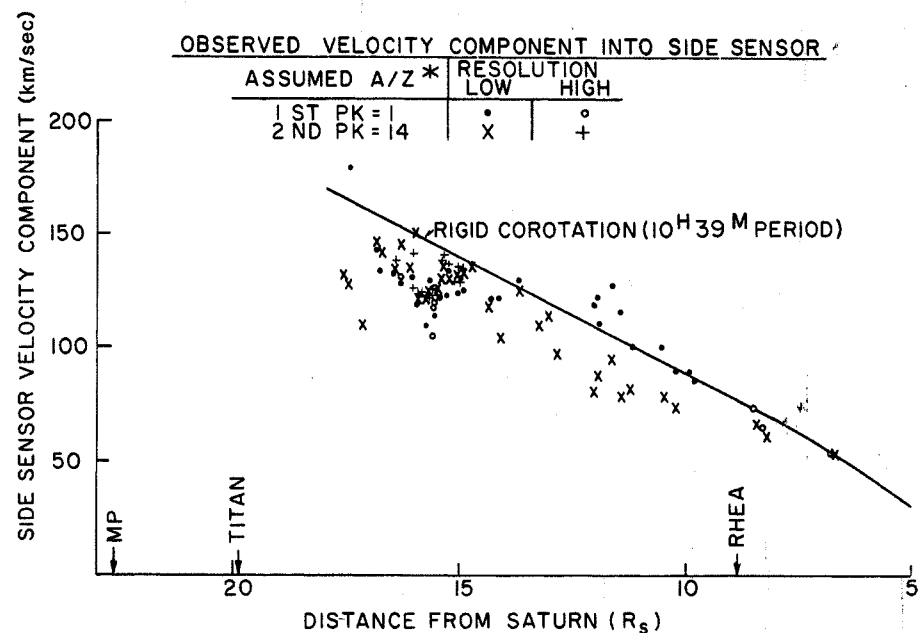
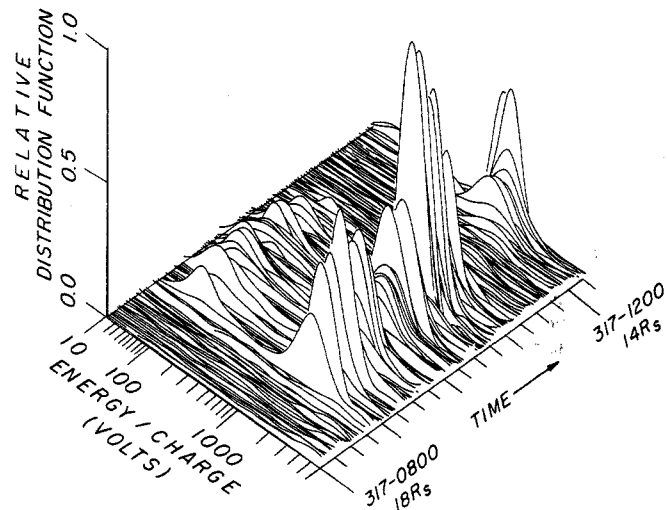


Fig. 4. The component of corotational velocity along the D sensor normal plotted against radial distance from Saturn. Ion peaks such as those shown in Fig. 3 are fitted by a convected Maxwellian. The convection velocities are obtained by assuming that the lower energy/charge peak is hydrogen and that the upper has $A/Z^* = 14$. A few points from analysis of higher resolution spectra are also shown. The velocities are compared with those expected for rigid corotation.

the higher resolution observations show the peak to be above that threshold after ~ 0200 . Because the sensor normal is $\sim 30^\circ$ to the equatorial plane, the threshold corresponds to a corotation velocity of ~ 60 km/sec for protons, well above the ~ 27 km/sec expected for rigid corotation. Thus, these observations may indicate the presence of heavier ions or field-aligned flow from the ionosphere. As the equatorial plane is approached,

the heavier mass peak becomes dominant, as would be expected if those ions were confined to the equatorial plane with a scale height of the order of $1 R_S$.

Configuration of the plasma sheet. The appreciable inclination of the Voyager 1 trajectory with respect to Saturn's equatorial plane permits exploration of the vertical as well as the radial distribution of plasma within the region of the magnetosphere where the magnetic field

is approximately dipolar. As a working hypothesis we assume that, within this region, the plasma distribution is at least approximately independent of longitude and local time, symmetrical about the equatorial plane, and without major temporal changes during the Voyager flyby.

We now use the variation of electron density (n_e) observed along the trajectory to investigate the dependence of n_e on the magnetic L shell location of the spacecraft and its position relative to the equatorial plane. We use the 15-minute averages of the measured electron number density shown in Fig. 1 and compare observations from the inbound and the outbound passes taken on the same L shell but at different distances (Z) from the equatorial plane. Figure 7A shows $|Z|$ versus L for the Voyager trajectory. (In view of the symmetry assumption, the absolute value $|Z|$ is shown; the actual trajectory prior in time to $L = 6.4$ lies below the equator.) Figure 7B shows the observed values of $n_e L^3$ as a function of $|Z|$ for different ranges of L identified by different symbols; the corresponding orbital locations in Fig. 7A are marked by the same symbols. (Observations of n_e for $L < 5$ affected by solar occultation have not been included.)

Although the L shell dependence cannot be uniquely determined, use of the quantity $n_e L^3$ organizes the data well and is theoretically advantageous since the plasma content per unit flux of a magnetic flux tube is proportional to N :

$$N = B_S \int (n_e/B) dl$$

where the integral is taken along the flux tube, dl is an element of path length along the flux tube, B is the field, and B_S is Saturn's dipole surface field at the equator (≈ 0.2 gauss). Near the equatorial plane, where most of the plasma is assumed to be confined, B is well approximated by B_S/L^3 . Then

$$N = \int n_e L^3 dZ$$

N is related to N_L , the tube content per unit L used in radial diffusion studies, by $2\pi N = L^2 N_L$.

We note the following features in Fig. 7B:

1) Within the range $5 < L < 7$, $n_e L^3$ shows no appreciable L dependence and has a Z dependence that is well approximated by a Gaussian

$$n_e L^3 \approx 2.4 \times 10^3 \exp[-(Z/0.93)^2] \quad (1)$$

with Z in R_S and n_e in cm^{-3} .

2) Within the range $7 < L < 12$, $n_e L^3$ follows the Gaussian profile (Eq. 1) as long as $|Z| \leq 1.2$ (the trajectory restricts these observations to $7 < L < 9$); at

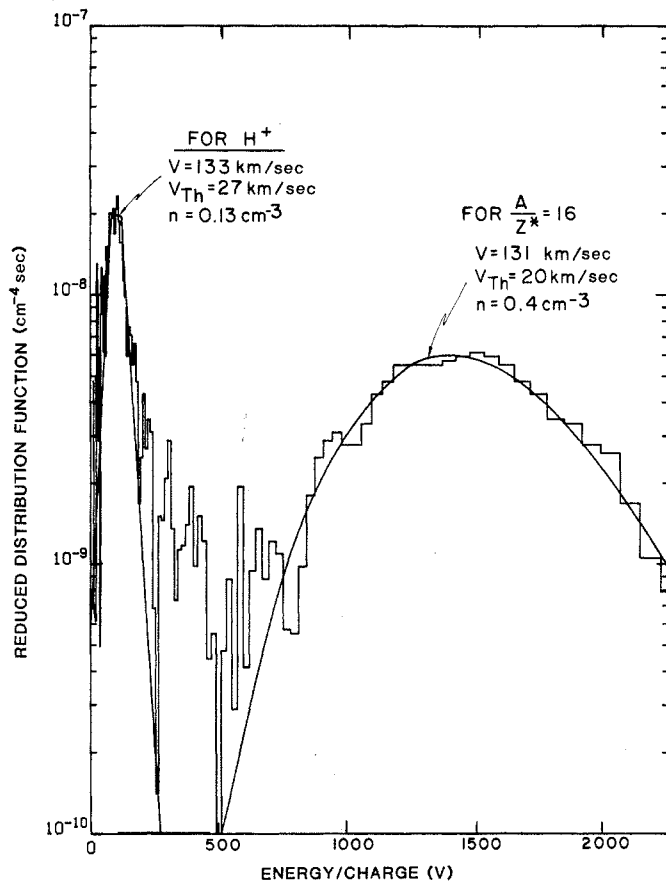
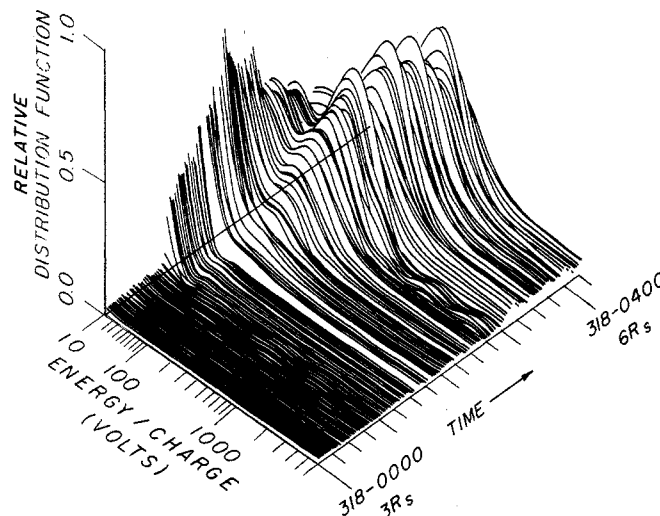


Fig. 5. A spectrum (0915, 12 November) in which analysis of the higher resolution mode, D sensor data is possible. The corotation velocity was 153 km/sec. The uncertainties in velocity are $\sim \pm 2$ km/sec. If the heavier peak were N^+ , its velocity would be ~ 139 km/sec. In all cases, the ions appear to be moving significantly slower than the 153 km/sec that the side sensor would be expected to observe. At this stage of the analysis, the fit to the higher energy/charge peak is consistent with either O^+ or N^+ ions.

Fig. 6. Sequence of low-resolution ion spectra taken from 0000 to 0416 on 13 November. The relative distribution functions are plotted as described for Fig 3. During this time interval the spacecraft rises from its lowest excursion in latitude almost to the equatorial plane. Note the increase in relative importance of the heavier mass component as the equatorial region is approached. The lower peak is caused either by corotating ions heavier than hydrogen or possibly by hydrogen of ionospheric origin.



greater distances from the equator, $n_e L^3$ is approximately constant, independent of both L and Z , up to $|Z| \approx 1.8$, above which it undergoes a sharp decrease which may be approximated as exponential:

$$n_e L^3 \approx 500 \quad \text{for } |Z| < 1.8 \quad (2a)$$

$$\approx 500 \exp[-(|Z| - 1.8)/0.24] \quad \text{for } |Z| > 1.8 \quad (2b)$$

The constant value of $n_e L^3$ given by Eq. 2a becomes equal to the Gaussian (Eq. 1) at $|Z| \approx 1.2$. (It should be noted that the inbound and the outbound trajectory both pass through $|Z| = 1.5$, $L = 9.7$, and the two density values agree to within 20 percent, supporting the assumption of axial symmetry.)

3) A nearly constant $n_e L^3$, equal to the value given by Eq. 2a, appears to persist at least up to $|Z| \approx 0.8$ in the range $12 < L < 14.5$, although here both the validity of the axial symmetry assumption and the use of a dipolar field are becoming questionable.

Plots were made as a function of latitude and similar variables rather than $|Z|$, but the extent to which the data points were organized was markedly inferior. The dependence on Z rather than latitude is particularly evident in the change from a nearly flat to a rapidly decreasing profile, which is observed on both inbound and outbound passes at nearly the same $|Z|$ (≈ 1.8) but different L (8 and 10.5, respectively). On the other hand, over the limited ranges of L used, $n_e L^3$ does not differ significantly from, say, $n_e L^4$.

A schematic model of the plasma sheet configuration consistent with the above results is sketched in Fig. 8. We identify two distinct structures, which we call the central plasma sheet and the extended plasma sheet. The central plasma sheet, observed between $L = 5$ and $L = 8$, has a density profile that decreases rapidly with distance Z away from the equatorial plane and can be represented as a Gaussian with a root-mean-square (RMS) width of $0.93 R_S$, an equatorial number density n (estimated by extrapolating Eq. 1 to $Z = 0$) of ≈ 20 to 7 cm^{-3} at $L = 5$ to 7 , and a flux tube content N of roughly $4 \times 10^3 R_S/\text{cm}^3$. The extended plasma sheet has a well-defined inner boundary at $L \approx 7$ and a density profile that is nearly flat to $|Z| \approx 1.8$ and decreases thereafter with a scale height of $0.24 R_S$. The equatorial density n and flux tube content N cannot be directly estimated, since Voyager observations of the extended plasma sheet do not reach below $|Z| = 0.8$, but simple ex-

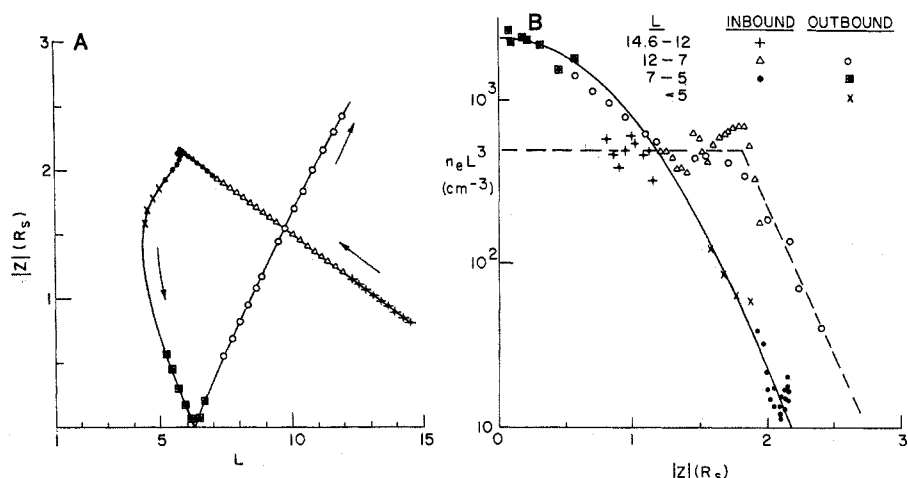


Fig. 7. Analysis of the plasma sheet electron data in terms of L shell location and distance from the equatorial plane. (A) Spacecraft L shell plotted against $|Z|$, the absolute value of its distance above the equatorial plane; (B) $n_e L^3$ plotted against $|Z|$. Data from times corresponding to particular spacecraft positions are indicated by common symbols on both curves.

trapolation of Eq. 2b to $Z = 0$ yields n ranging from $\sim 1 \text{ cm}^{-3}$ at $L = 8$ to $\sim 0.3 \text{ cm}^{-3}$ at $L = 12$ and a roughly constant $N \approx 2 \times 10^3 R_S/\text{cm}^3$. An outer boundary of the extended plasma sheet cannot be determined, since the symmetry and field geometry assumptions of the analysis become inapplicable, but the data contain no clear indication of a major change at least out to 17 to $18 R_S$.

Our crude estimates of the equatorial number density are reasonably consistent with the radial ion density profile observed near the equatorial plane by Pioneer 11 (10). We are thus encouraged to assume that the plasma sheet configuration did not change drastically between the Pioneer and Voyager flybys and to combine the results of both into a consistent picture. We identify the central plasma sheet with the torus of enhanced ion densities observed by Frank *et al.* (10) between 4 and $7.5 R_S$; accordingly, the radial extent of the central plasma sheet, not determined by Voyager because of trajectory limitations, is probably bounded by $L = 4$ and $L \approx 8$. The density decrease observed in the equatorial plane beyond $L \approx 7$ to 9 appears to be due to a sudden increase of plasma sheet thickness with relatively little change of flux tube content. The $L \approx 7$ sheet, where the inner edge of the extended plasma sheet is located, also coincides or nearly coincides with the inner edge of the atomic hydrogen torus (11) and with several changes of energetic particle properties described as the transition from the outer magnetosphere to the slot region (12).

At present, we can only speculate on the sources of plasma within the two plasma sheet structures. Their flux tube contents are sufficiently similar (the dif-

ference of a factor of 2 is well within the observational uncertainties) that no possibility can be ruled out on the basis of flux tube content arguments alone; either one may, in principle, be formed by diffusion from the other, or each may derive from a separate source. Sputtering from ring particle surfaces and possible inputs from Dione and Tethys, as suggested by Frank *et al.* (10), is a plausible source for the central plasma sheet. The extended plasma sheet may derive partly from Saturn's ionosphere, from ionization of the neutral hydrogen torus, or from inward diffusion of Titan-associated plasma. Important aspects to consider in studying the source problem will be ion composition, radial variation of temperature, and relation of vertical confinement distance to pressure anisotropy and temperature.

Interaction between Titan and the magnetospheric plasma. Plasma observations during the close approach of Voyager 1 to Titan are summarized in Fig. 9. The major observational features include the following. (i) The electron number density is enhanced to a mean value of about 0.5 cm^{-3} , compared to an ambient density (observed in the magnetosphere near Titan but away from the interaction region) of 0.07 to 0.1 cm^{-3} . One measurement shows a number density of 1.5 cm^{-3} , but in view of the 96-second spacing between the 4-second-long individual measurements, it is not possible to determine from our data alone either the duration or the maximum value of this localized enhancement. The overall density enhancement extends over nearly the full geometrical-ly predicted Titan wake in a corotating magnetospheric flow, is preceded by a slow density buildup and followed by a

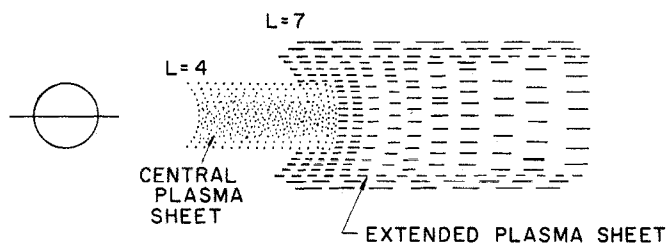
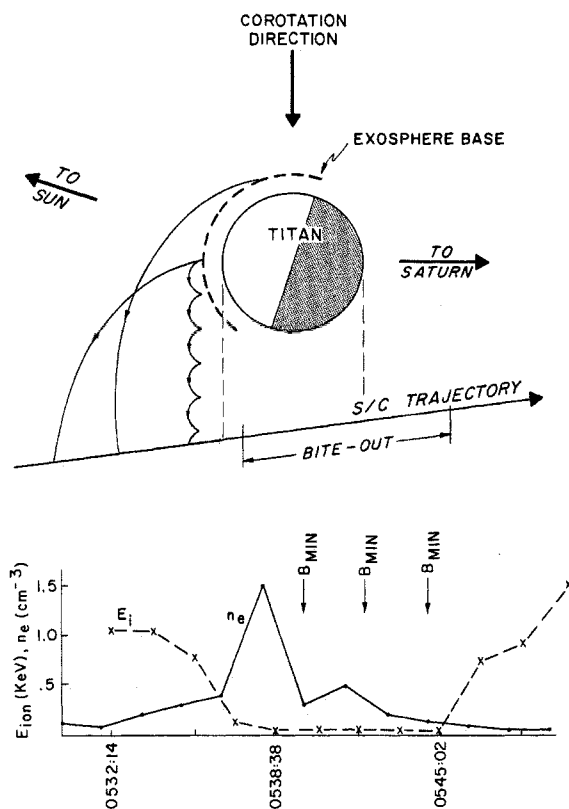


Fig. 8. Schematic model of the plasma sheet configuration.

somewhat faster density falloff, and is accompanied by a decrease of electron temperature. (ii) A sharp decrease or "bite-out" occurs in the intensity of electrons with energies above 700 eV. This region is indicated in Fig. 9, and the electron distribution functions throughout the interaction are shown in Fig. 10. The bite-out is considerably inside the position of the geometrical wake of Titan (that is, radially inward relative to Saturn) and approximately coincides with the location of the tail-like magnetic field structure observed by Ness *et al.* (13). (iii) The mean energy/charge of the plasma ions throughout the interaction region is reduced well below the ~ 1 keV typical of the ambient magnetospheric plasma. As shown in Fig. 9, the ion energy begins to decrease with the beginning of the electron density enhance-

ment, becomes as low as some tens of electron volts within the bite-out region, and begins to increase again only when the electron density has decreased almost to the ambient level. The region of low energies is approximately centered on the middle of the bite-out (and of the tail-like magnetic field structure), but extends significantly beyond it on either side. Within the bite-out, the ions are observed predominantly by the D sensor, which faces approximately toward Titan; their energy spectra show a sharp low-energy peak which, if interpreted as representing a bulk speed, implies a flow velocity away from Titan of approximately $50/\sqrt{A}$ km/sec. Strictly speaking, this represents an upper limit to the velocity, since the tail-like magnetic field within the wake allows, in principle, a counterflow toward Titan that would lie

Fig. 9. Plasma observations in the vicinity of Titan's magnetospheric wake. The mean energies of the ions are plotted at the times corresponding to the low-resolution mode observations. Electron densities, n_e , are plotted at times halfway between the times of observation of the low- and high-energy portions of the spectra (since the two portions are taken 48 seconds apart). The cycloidal paths of N^+ and H^+ ions from Titan's exosphere are shown at proper scale for magnetospheric plasma moving 200 km/sec, if it is assumed that ions are picked up by a magnetic field of ~ 5 nT perpendicular to the plane of the figure (13). (In reality, the slowing down of the plasma and the creation of a nonuniform electric field will significantly modify the trajectories.) The bite-out region, where the high-energy electrons are depleted (see Fig. 10), is indicated. Its boundaries correspond to times of measurement of the higher-energy portion of the appropriate electron spectra. The locations of minima in the observed field (13) are also indicated. The dotted lines show the position of the geometrical corotational wake.



outside our instrument's field of view; however, if the interpretation given below is correct, such a counterflow is most improbable.

The Titan wake displays an intrinsic asymmetry and is not merely rotated from some expected orientation. The central structure of the wake, defined by the tail-like magnetic field and identified in our data by the > 700 eV electron bite-out, is displaced sideways relative to the increase in electron density; the electron density is enhanced primarily on the side of the wake away from Saturn. This asymmetry, as well as most other features of the plasma observations, can (at least qualitatively) be accounted for by a model of the interaction between Titan and the magnetosphere in which exospheric neutral particles from Titan become ionized and are subsequently accelerated in the $V \times B$ electric field associated with the corotational flow of magnetospheric plasma; one speaks of atmospheric ions being "picked up" by the flowing plasma. Such models have been discussed by Cloutier *et al.* (14), Hartle *et al.* (15), and others, primarily in connection with solar wind flow past Venus and past a comet.

Single trajectories of heavy (N^+) and light (H^+) ions picked up by the corotational flow of ~ 200 km/sec at Titan are sketched (correctly scaled) in Fig. 9. The initial acceleration is along the corotational electric field, which points away from Saturn, but deflection by the magnetic field soon leads to the familiar cycloidal motion. As long as the ion gyroradius exceeds the vertical scale height of the exosphere, only on the outer side of Titan (facing away from Saturn) can an appreciable number of ions be picked up and carried away by the flow. Ions produced on the inner side are mostly intercepted by the atmosphere. Even on the outer side, the column density traversed by the ions depends critically on the gyroradius and hence on the mass and energy of the ion. For example, a proton whose guiding center is near the exobase will traverse an amount of material at least equal to that determined by its Chapman distance (16): for a Titan exobase at 3900 km, a scale height of 80 km, and a neutral density at the exobase of 2×10^8 cm^{-3} (11), the column density of nitrogen is $\sim 10^{16}$ cm^{-2} , comparable to the interaction length for the ions. The asymmetric electron density enhancement may be produced by addition of ions and electrons to the plasma through this process.

As plasma flows past Titan, it is ex-

pected to slow down as a result of mass loading by the picked-up ions. The observed reduction of ion energy in and near the wake region presumably is related to this velocity decrease. A more detailed analysis of the complex spectra observed in all four sensors is needed to identify precisely the effects of velocity changes and of non-Maxwellian distributions expected for ions picked up by the field.

Finally, the bite-out region is associated with magnetic field lines stretched out into a tail-like shape, presumably because the plasma on part of such a line is greatly slowed down by interaction with Titan while the remainder of the line is still carried onward by corotation; the field line is thus connected to Saturn's magnetosphere and to Titan's ionosphere. Magnetospheric electrons can move readily along these field lines and be lost to the atmosphere by scattering and absorption, which become more important at higher energies. However, electrons lost from the magnetosphere must be replaced by cold ionospheric electrons, since the ions cannot be lost at a comparably high rate (the observations, in fact, indicate an ion flow away from Titan in this region and, therefore, an ion source from Titan's ionosphere or atmosphere); the net result of this process is a reduction of the magnetospheric electron population at high energies and an increase at low energies. Similar effects have been observed on magnetic field lines downstream of Venus (17, 18).

The process described above, which acts preferentially to remove low-mass or lower energy ions, enhances the effects of scattering and absorption for higher energy electrons on the outer side of Titan. Near the exobase, electrons of energy ~ 700 eV have gyroradii comparable to the local scale height. Since electrons move inward as they gyrate, those above this energy will be preferentially scattered or absorbed by Titan's atmosphere and replaced by cold ionospheric electrons. Qualitatively at least, this mechanism appears to explain the bite-out. Although removal of high-energy electrons is partially responsible for the large decrease in electron temperature observed in the Titan wake, a significant part of the temperature decrease must be associated with the addition of cold electrons to balance the charge of ions picked up at Titan.

A conventional standing bow shock at Titan would certainly have been detected by this experiment and by the magnetometer. Nevertheless, no evidence for a fast-mode shock is found in the data,

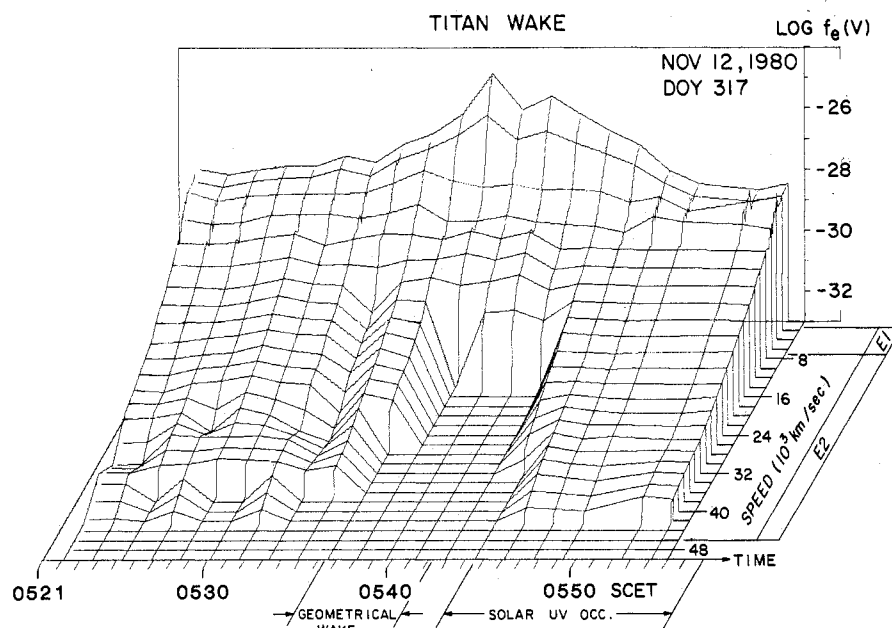


Fig. 10. The observed electron distribution functions in the Titan wake region. Energy increases toward the viewer. In this figure, an individual distribution is plotted at a time corresponding to measurement of its lower energy portion.

which are completely consistent with subsonic flow of the magnetospheric plasma around Titan. The flow is, however, supersonic with respect to the ion sound speed, and some evidence for a slow-mode shock has been reported (19). In this case, the plasma temperature should increase across the discontinuity; our results show a marked decrease in electron temperature and probably a decrease in ion temperature. Final resolution of this question should be available after a more extensive analysis of the positive ion data.

In the region of strong interaction, where ions newly picked up from the exosphere of Titan are an important component of the observed plasma, significant effects associated with the different gyroradii of electrons and positive ions might be expected. In particular, charge neutralization (time average) is likely to involve electron and ion plasma oscillations, which may have been observed by the plasma wave experiment (19). It can be shown that the ion plasma oscillations will not be damped over the time interval separating their origin and their measurement. Because of their gyro motion, these ions are warm and therefore produce a wide spectrum of frequencies reflecting their effective temperatures. If the composition of picked-up ions changes along the trajectory of the spacecraft, the average frequency of the ion oscillations will vary also. This effect may have been observed (19).

Titan as a plasma source for the mag-

netosphere. If the interpretation of Titan wake observations given above is correct, Titan constitutes a significant source of plasma for the outer magnetosphere. To obtain an order-of-magnitude estimate of the source strength, we approximate the area of plasma injection by a circular disk whose diameter is equal to the width of the observed electron density enhancement region (~ 9000 km ≈ 1.6 Titan diameters) and take the mean number density (0.5 cm $^{-3}$) and assumed ion flow velocity (50 km/sec) observed near the center of the Titan wake as representative. The resulting estimated source strength (total rate of ion injection from the Titan wake into the magnetosphere) is approximately 2×10^{24} sec $^{-1}$. We emphasize again that this value is uncertain and should be treated as a representative order of magnitude only.

The injected plasma is expected to contain hydrogen and heavier ions (in particular N $^+$). Corotational motion will extend this plasma azimuthally into a toruslike structure. The detailed density distribution depends on the transport and loss processes, which are still poorly known. A potentially important loss process is escape of the torus plasma down the magnetotail as the corotational motion brings the flux tubes loaded with plasma into the nightside of the magnetosphere, where the confining external pressure of the solar wind decreases and the magnetic tension may no longer be adequate to maintain the plasma in cor-

tation. An analogous escape process has been extensively discussed for the magnetosphere of Jupiter. This loss process may operate either as a more or less steady planetary wind (20–22) or as a time-dependent and intermittent occurrence (23, 24).

Initially, the plasma emitted by Titan is confined to a long and narrow wake in the magnetospheric flow that can be compared to the plume from a smokestack in the wind. This plasma plume, while remaining attached to Titan at one end, can acquire a highly contorted, meandering shape as a consequence of stochastic radial motions of the magnetospheric plasma associated, for example, with expansions and contractions of the entire magnetosphere in response to changing solar wind pressure. The plume may also, if it remains identifiable for a time longer than a planetary rotation, wrap itself around the entire magnetosphere and return to the vicinity of Titan. It is thus conceivable that the spacecraft trajectory may intercept the plume more than once. In fact, within a distance of several R_S about Titan, we observe several localized enhancements of electron density accompanied by decreases of electron temperature, similar in character to the density enhancement observed on crossing the Titan wake, but of considerably reduced amplitude. That these density increases represent multiple crossings of the extended plasma plume from Titan is possible, but not yet firmly established. If they are plasma plume crossings, two models may be considered: (i) the plume may be long-lived and identifiable after many planetary rotation periods, so that the multiple crossings are associated with multiple wrapping of the plume around Saturn and the relative radial distances carry a record of past radial motions of the magnetosphere; or (ii) the plume may be short-lived, and the multiple crossings result from localized distortions or motions, possibly analogous to similar effects observed in association with the wake of Ganymede (25, 26). Further analysis is needed to decide between these possibilities.

Atomic hydrogen torus as a plasma source. An additional source of plasma for the magnetosphere is provided by ionization of neutral atoms gravitationally trapped in the Saturn system. A ring of atomic hydrogen around the orbit of Titan was proposed long ago (27). The Voyager ultraviolet experiment observations (11) have shown that there exists a torus of neutral atomic hydrogen much more extensive than was anticipated. Results of Lyman α scans indicate a

washer-shaped region of atomic hydrogen extending from a radial distance of $23 R_S$ inward to about $7 R_S$, with an approximately constant vertical extent of $\pm 1 R_S$ away from the equatorial plane and an approximately constant density of 10 cm^{-3} . To estimate a source strength, we adopt a photoionization time of 2×10^8 seconds, an electron impact ionization time of 3×10^7 seconds [for $n_e = 1 \text{ cm}^{-3}$ and $T_e \approx 100 \text{ eV}$ (28)], and a density model $n_e \approx 0.1 + (500/L^3) \text{ cm}^{-3}$ (see previous discussion of extended plasma sheet). With the cited dimensions and density of the hydrogen torus, we then calculate a total source strength of 6×10^{24} ions per second added to the magnetospheric plasma, with nearly equal contributions from electron impact and photoionization. This is of the same order of magnitude as the Titan source. The hydrogen torus, unlike Titan, contributes only protons (unless as yet undetected heavier species are present in appreciable amounts within the torus), and the source is spatially distributed rather than localized. The ionization rate per unit volume, calculated from our model, increases with decreasing radial distance and, relative to its value near Titan's orbit ($L = 20$), is five times and seven times larger at $L = 10$ and $L = 7$, respectively. The volume contained between $L = 22$ and $L = 18$ contributes 30 percent of the total.

H. S. BRIDGE

J. W. BELCHER, A. J. LAZARUS

S. OLBERT, J. D. SULLIVAN

F. BAGENAL, P. R. GAZIS

*Center for Space Research and
Department of Physics,
Massachusetts Institute of
Technology, Cambridge 02139*

R. E. HARTLE

*Laboratory for Planetary Atmospheres,
Goddard Space Flight Center,
Greenbelt, Maryland 20771*

K. W. OGILVIE

J. D. SCUDDER, E. C. SITTLER

*Laboratory for Extraterrestrial Physics,
Goddard Space Flight Center*

A. EVIATAR*

G. L. SISCOE

*Department of Atmospheric Sciences,
University of California,
Los Angeles 90024*

C. K. GOERTZ

*Max-Planck-Institut für Aeronomie,
D-3411, Katlenburg-Lindau 3,
Federal Republic of Germany, and
University of Iowa, Iowa City 52242*

V. M. VASYLIUNAS

*Max-Planck-Institut für Aeronomie,
D-3411, Katlenburg-Lindau 3*

References and Notes

- H. S. Bridge, J. W. Belcher, A. J. Lazarus, J. D. Sullivan, R. L. McNutt, F. Bagenal, J. D. Scudder, E. C. Sittler, G. L. Siscoe, V. M. Vasyliunas, C. K. Goertz, C. M. Yeates, *Science* **204**, 987 (1979).
- H. S. Bridge *et al.*, *Space Sci. Rev.* **21**, 259 (1977).
- H. C. Howe and J. H. Binsack, *J. Geophys. Res.* **77**, 3334 (1972).
- J. H. Wolfe *et al.*, *Science* **207**, 403 (1980).
- J. D. Scudder, E. C. Sittler, H. S. Bridge, *J. Geophys. Res.*, in press.
- E. J. Smith, L. Davis, Jr., D. E. Jones, P. J. Coleman, Jr., D. S. Colburn, P. Dyal, *Science* **207**, 407 (1980).
- M. H. Acuña and N. F. Ness, *ibid.*, p. 444.
- M. L. Kaiser, M. D. Desch, J. W. Warwick, J. B. Pearce, *ibid.* **209**, 1238 (1980).
- R. L. McNutt, Jr., J. W. Belcher, J. D. Sullivan, F. Bagenal, H. S. Bridge, *Nature (London)* **280**, 803 (1979).
- L. A. Frank, B. G. Burek, K. L. Ackerson, J. H. Wolfe, J. D. Mihalov, *J. Geophys. Res.* **85**, 5695 (1980).
- A. L. Broadfoot, B. R. Sandel, D. E. She-mansky, J. B. Holberg, G. R. Smith, D. F. Strobel, J. C. McConnell, S. Kumar, D. M. Hunten, S. K. Atreya, T. M. Donahue, H. W. Moos, J. L. Bertaux, J. E. Blamont, R. B. Pomphrey, S. Linick, *Science* **212**, 206 (1981).
- J. H. Trainor, F. B. McDonald, A. W. Scharadt, *ibid.* **207**, 421 (1980).
- N. F. Ness, M. H. Acuña, R. P. Lepping, J. E. P. Connerney, K. W. Behannon, L. F. Burlaga, F. M. Neubauer, *ibid.* **212**, 211 (1981).
- P. A. Cloutier, R. E. Danielle, Jr., A. J. Dessler, P. W. Hill, *Astrophys. Space Sci.* **55**, 93 (1978).
- R. E. Hartle, K. W. Ogilvie, C. S. Wu, *Planet. Space Sci.* **21**, 2181 (1973).
- E. J. McCartney, *Optics of the Atmosphere* (Wiley, New York, 1976), p. 110.
- C. M. Yeates, K. W. Ogilvie, G. L. Siscoe, *J. Geophys. Res.* **83**, 1524 (1978).
- H. S. Bridge, A. J. Lazarus, J. D. Scudder, K. W. Ogilvie, R. E. Hartle, J. R. Asbridge, S. J. Bame, W. C. Feldman, G. L. Siscoe, *Science* **183**, 1293 (1974).
- D. A. Gurnett, W. S. Kurth, F. L. Scarf, *ibid.* **212**, 235 (1981).
- F. C. Michel and P. A. Sturrock, *Planet. Space Sci.* **22**, 1501 (1974).
- T. W. Hill, A. J. Dessler, F. C. Michel, *Geophys. Res. Lett.* **1**, 3 (1974).
- S. M. Krimigis, T. P. Armstrong, W. I. Axford, C. O. Bostrom, C. Y. Fan, G. Gloeckler, L. J. Lanzerotti, E. P. Keath, R. D. Zwickl, J. F. Carbary, D. C. Hamilton, *Science* **206**, 977 (1979).
- T. W. Hill and F. C. Michel, *Rev. Geophys. Space Phys.* **13**, 967 (1975).
- J. F. Carbary, T. W. Hill, A. J. Dessler, *J. Geophys. Res.* **81**, 5189 (1976).
- H. S. Bridge, J. W. Belcher, A. J. Lazarus, J. D. Sullivan, F. Bagenal, R. L. McNutt, Jr., K. W. Ogilvie, J. D. Scudder, E. C. Sittler, V. M. Vasyliunas, C. K. Goertz, *Science* **206**, 972 (1979).
- N. F. Ness, M. H. Acuña, R. P. Lepping, L. F. Burlaga, K. W. Behannon, F. M. Neubauer, *ibid.*, p. 966.
- T. R. McDonough and N. M. Brice, *Icarus* **20**, 136 (1973).
- R. W. Carlson, D. L. Matson, T. V. Johnson, *Geophys. Res. Lett.* **2**, 469 (1975).
- This report is the result of a team effort by many individuals who contributed their special talents for long hours. We are deeply indebted to them. We especially thank E. J. Franzgrote, O. Divers, R. Parker, and M. Nelson at Jet Propulsion Laboratory for their assistance in encounter planning and operations; J. Boughan, A. Bowes, J. Binsack, M. Carracino, G. Gordon, Jr., P. Milligan, M. Terkoski, S. Skinner, R. Tokar, and R. DiSanto at Massachusetts Institute of Technology; and T. Volmer, P. Harrison (of Computer Science Corporation), F. Hunsaker, W. Mish, and T. Carleton at Goddard Space Flight Center for their support of the encounter efforts. Our interpretation of data near Titan has been aided by early discussions and comparison of data with the magnetometer experimenters, N. F. Ness and his co-investigators. This work was sponsored by the National Aeronautics and Space Administration and performed under contract 953733 to Jet Propulsion Laboratory.
- * On leave from the Department of Geophysics and Planetary Science, Tel-Aviv University, Ramat-Aviv, Israel.

9 February 1981